This document is the accepted manuscript version of the following article:
Decking, W., Abeghyan, S., Abramian, P., Abramsky, A., Aguirre, A., Albrecht, C., … Zybin, D. (2020). A MHz-repetition-rate hard X-ray free-electron laser driven by a superconducting linear accelerator. Nature Photonics, 14(6), 391-397.
https://doi.org/10.1038/s41566-020-0607-z

A MHz-repetition-rate hard X-ray free-electron laser driven by a superconducting linear accelerator

The European XFEL is a hard X-ray free-electron laser (FEL) based on a high-electron-energy superconducting linear accelerator. The superconducting technology allows for the acceleration of many electron bunches within one radio-frequency pulse of the accelerating voltage and, in turn, for the generation of a large number of hard X-ray pulses. We report on the performance of the European XFEL accelerator with up to 5,000 electron bunches per second and demonstrating a full energy of 17.5 GeV. Feedback mechanisms enable stabilization of the electron beam delivery at the FEL undulator in space and time. The measured FEL gain curve at 9.3 keV is in good agreement with predictions for saturated FEL radiation. Hard X-ray lasing was achieved between 7 keV and 14 keV with pulse energies of up to 2.0 mJ. Using the high repetition rate, an FEL beam with 6 W average power was created.

Over the past decade, hard X-ray free-electron lasers (FELs) have been proposed and established as light sources for X-ray research[1–5]. The successful design, construction and operation of these facilities is based on theoretical, experimental and technological developments in FEL and accelerator physics from the early 1980s until now (see the review papers in refs. [6–8] and references therein). Seminal studies refer to the generation of X-ray radiation by an electron beam during a single pass of an undulator, where the amplification process develops from the shot noise in the electron beam[9–11] (later, this amplifier configuration was named a self-amplified spontaneous emission (SASE) FEL[12]). From 1998, we observed a very rapid development of SASE FEL facilities operating in the infrared (for example, the VISA experiment in 1998[13]), visible (LEUTL, in 2000[14]) and soft X-ray (FLASH, in 2000[15]) regimes, with the first X-ray user facility, the Free Electron LASer in Hamburg (FLASH), put into operation in 2005[16].

The completely new capabilities of these facilities and their enormous scientific success are driving a huge demand for access. This can be accommodated in part by high-repetition-rate facilities serving several scientific instruments in parallel. The European X-Ray Free-Electron Laser Facility (European XFEL) is an international research infrastructure built in the Hamburg area of Germany. Twelve nations have contributed to its construction (Denmark, France, Germany, Hungary, Italy, Poland, Russia, Slovenia, Spain, Sweden, Switzerland and the United Kingdom). The European XFEL accelerator is based on superconducting technology developed in the framework of the TESLA collaboration by an international consortium centred around Deutsches Elektronen-Synchrotron (DESY)[17]. After the first observation of lasing in the VUV regime at the TESLA Test Facility (now FLASH)[15], a hard X-ray FEL was proposed as part of a linear collider and later transformed into a standalone facility[18]. The realization of the project as an international research infrastructure[4] started officially in 2009 with the foundation of European XFEL GmbH and the start of civil construction.

The complete facility is constructed underground, ~6 to 38 m below surface level, in several 4.6- and 5.3-m-diameter tunnels with a total length of ~5.3 km (Fig. 1). The 50-m-long injector occupies the lowest level of a seven-storey underground building that also serves as the entry shaft to the main linear accelerator (linac) tunnel. The next access point to the tunnel system is ~2 km downstream at the bifurcation point into the beam distribution lines. The beam distribution provides space for five FEL undulators (three having been installed initially), each pointing into a separate tunnel, so that a fan of five almost parallel tunnels with a lateral distance of 17 m between beams enter the experiment hall 3.3 km from the electron source. The civil construction of the tunnels ended in 2013 and infrastructure installation continued until 2014. By the end of 2016, the accelerator installation was complete (Fig. 2) and its commissioning and operation began. Installation of photon components and experiment set-up proceeded beamline by beamline, with the first completed in summer 2017. The first experiments by user groups started in September 2017, leading to initial scientific results[19,20]. Installation of the second and third beamlines was completed in the summer and autumn of 2018, respectively.

The European XFEL uses the SASE FEL principle, where radiation is produced by the electron beam during a single pass of an undulator[9–11]. The amplification process develops from the shot noise in the electron beam, and strong, coherent, narrowband radiation is generated near the resonant wavelength, $\lambda = \lambda_w(1+K^2)/(2\gamma^2)$, where γ is the relativistic Lorentz factor, λ_w is the undulator period, $K = eH_w\lambda_w/(2\pi mc)$ is the undulator parameter, H_w is the root mean square (r.m.s.) on-axis magnetic field strength of the undulator, c is the speed of light, and m and e are the mass and charge of the electron. The main characteristics of the X-ray FEL (field gain length L_g, saturation length L_{sat}, saturation efficiency $\eta = W_{rad}/W_{eb}$, coherence time at saturation τ_c and spectrum bandwidth σ_ω) are well estimated in terms of the FEL parameter ρ and the number of cooperating electrons $N_c = I/(e\rho\omega)$ (refs. [21–23]):

$$L_g \approx \frac{\lambda_w}{4\pi\rho}, L_{sat} \approx \frac{\lambda_w}{4\pi\rho}\left(3+\frac{\ln N_c}{\sqrt{3}}\right), |\eta \simeq \rho|, \tau_c \simeq \frac{1}{\rho\omega}\sqrt{\frac{\pi \ln N_c}{18}}, \sigma_\omega = \sqrt{\pi}/\tau_c$$

The FEL parameter ρ is given by[21] $\rho = \left(\lambda_w^2 j_0 K^2 A_{jj}^2/(16\pi I_A \gamma^3)\right)^{1/3}$,

where j_0 is the beam current density, $I_A = mc^3/e \simeq 17$ kA is the Alfven current, and A_{jj} is a coupling factor with a value close to 1.

A full list of authors and their affiliations appears online. ✉e-mail: winfried.decking@desy.de

Fig. 1 | Bird's-eye view of the facility showing the location of the tunnel buildings in the urban area of the city of Hamburg. The injector is on the right on the DESY campus, while the experiment hall and headquarters of the European XFEL are on the left in the federal state of Schleswig-Holstein. Note the fan of five photon beamlines entering the experiment hall. Credit: European XFEL / Luftaufnahmen: FHH, Landesbetrieb Geoinf. und Vermessung

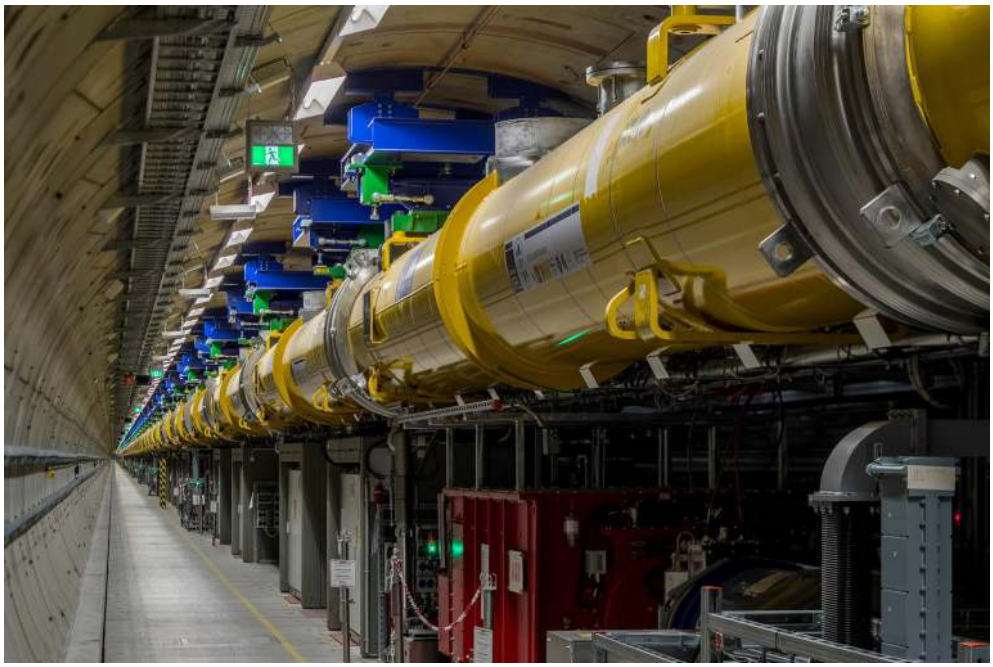

Fig. 2 | View along the almost 1-km-long superconducting linac section L3, which accelerates the beam after the last bunch compression stage from 2.5GeV up to 17.5GeV. Note that the accelerator is supported from the tunnel ceiling, while the complete infrastructure (high-power radio-frequency (RF), electronics and auxiliaries) is installed on the tunnel floor for easy maintenance and access. Credit: DESY / Dirk Nölle

The typical amplification bandwidth of the X-ray FEL is of the order of 0.1%. The electron beam in an X-ray FEL transfers enormous peak power. For typical X-ray FEL parameters (electron energy of 17.5 GeV, peak current of 5 kA and bunch charge of 0.5 nC), the peak power in the electron beam, W_{eb}, is ~100 TW, and the kinetic energy of electrons is ~10 J. The conversion efficiency of the kinetic energy of electrons to the light is of the order of the amplification bandwidth; thus, the peak power of the X-ray radiation, W_{rad}, is in the multi-GW range and radiation pulse energies are in the few-mJ range.

The unique feature of the European XFEL is the capability of the superconducting linac to accelerate trains of many (up to 2,700) electron bunches within one 600-µs-long RF pulse. Using a 10 Hz RF pulse repetition rate, up to 27,000 electron bunches, and thus photon pulses, can be produced each second. The working point for the pulsed superconducting linac is optimized in terms of pulse duration, accelerating gradient and cryo load. Future projects[24,25] aim for continuous-wave operation and thus an equidistant bunch structure. This is possible through recent advances in the treatment of superconducting cavities but will nevertheless come at the price of reduced accelerating gradient and increased cryogenic load.

Electron bunch charges can be varied from 20 to 1,000 pC (ref. [26]), with resulting bunch lengths after compression ranging from 3 to 150 fs full-width at half-maximum (FWHM)[27]. With different linac energies ranging from 8 to 17.5 GeV and variable-gap undulators, photon energies from 0.25 to 25 keV can be covered. A sophisticated electron-bunch distribution system allows us to distribute bunches

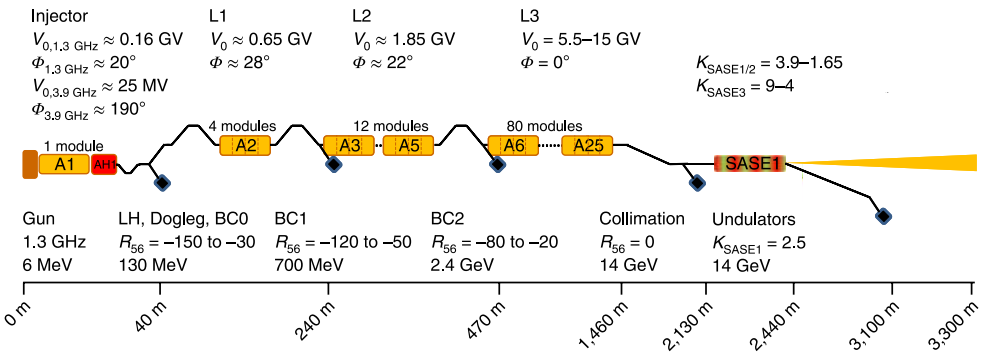

Fig. 3 | Schematic layout of the European XFEL accelerator and photon beam transport. The layout is that used in lasing in the initial operation phase. LH, laser heater; BC, bunch compressor. Figure adapted from ref. [46], under a Creative Commons licence (https://creativecommons.org/licenses/by/3.0/).

into each undulator beamline individually, thus enabling the simultaneous operation of several experiments.

Here we report on the performance of the European XFEL with up to 5,000 bunches per second at an electron energy of 14 GeV, serving the SASE1 undulator and producing SASE FEL radiation at ~9 keV as obtained until end of 2018.

Results

Injector. The photo-injector consists of a normal-conducting 1.3 GHz 1.6-cell cavity[28] with a Cs_2Te photocathode inserted at the back plane, which is illuminated by a Nd:YLF laser operating at 1,047 nm and converted to ultraviolet wavelength in two conversion stages. The laser was provided by the Max Born Institute, Berlin. A second laser was constructed as a back-up with reduced specifications with respect to the achievable pulse length. This laser is presently used as the primary injector laser because of its capability to be connected to the optical synchronization system, leading to a higher timing accuracy during operation. The photo-injector has been conditioned and characterized at the Photo Injector Test Facility at DESY in Zeuthen (PITZ), where a projected normalized emittance of 0.8 mm mrad has been demonstrated at a bunch charge of 500 pC (ref. [29]). This was achieved at the design cavity gradient of 60 MV m^{-1}, or, taking into account the required high duty cycle, at an average power of 50 kW. The photo-injector was operated at a reduced gradient between 52 and 58 MV m^{-1} at the European XFEL to enhance availability during commissioning and early operation.

The photo-injector is followed by a superconducting 1.3 GHz accelerating module and a third harmonic linearizer consisting of a 3.9 GHz module—also superconducting—that contains eight nine-cell cavities[30]. A laser heater[31], a diagnostic section and a high-power dump complete the injector. The diagnostic section allows the measurement of projected and slice emittance along the bunch train. This is achieved by a combination of a transverse deflecting cavity and several kickers and screens[32]. The transverse deflecting cavity deflects electrons within a bunch differently, depending on their longitudinal position. This allows measurement of the transverse emittance of individual bunch slices. The longitudinal dimensions of the bunch are determined from the projection of the deflected bunch profile, and slice energy spread can be measured in a dispersive beamline before the electron beam dump.

With the given set-up, projected emittances of 1.2 mm mrad (compared to the specified 1.5 mm mrad) and slice emittances of 0.6 mm mrad were observed. Most notable is the capability to also measure beam parameters along the bunch train, which helps to set up equal lasing conditions along the bunch train[33].

Bunch compression. A three-stage system for bunch compression is used, separating the linac into three parts, called L1, L2 and L3 (Fig. 3). All magnetic chicanes are tunable within a wide range to allow for flexible compression scenarios, for example balancing peak current and arrival time stability with accelerator performance. Tuning is achieved by means of large-pole-width dipole magnets and accordingly wide (400 mm) vacuum chambers. Diagnostic stations similar to the one in the injector are placed after the second and third compression stages.

During first operation in 2017, the accelerator was run at a bunch charge of 500 pC. The bunch length measurement was resolution-limited at that time, and the bunch length was estimated to be of the order of 50 fs r.m.s. Beginning in 2018, the bunch charge was reduced to 250 pC, and functional bunch length measurements confirmed a simulated pulse duration of ~20 fs (r.m.s., Gaussian fit; see Table 1).

Table 1 | Key performance parameters of the European XFEL accelerator and SASE1 FEL undulator

Parameter	Unit	Design	At first lasing and operation
Energy range	GeV	8–17.5	14
Bunch charge	pC	20–1,000	250, 500
RF pulse repetition rate	Hz	10	10
RF pulse length	μs	600	600
No. of bunches within the RF pulse		1–2,700	1–500
Peak current	kA	3–5	5
Bunch length (r.m.s.)		3–150	20, <50
Norm. slice emittance	mm mrad	0.4–1.0	<0.6
Undulator active length	m	175	140
Period length, λ	mm	40	40
K parameter		3.9–1.65	2.9
Undulator average β function	m	15–60	32

Accelerator. The superconducting linac consists of 96 accelerator modules built with TESLA technology. Groups of four modules, with eight nine-cell cavities each, are fed by one 10 MW multi-beam klystron. The accelerator modules are suspended from the tunnel ceiling (Fig. 2), while the complete RF infrastructure (klystrons, pulse transformers and low-level radio-frequency (LLRF) electronics) is installed below the modules. The modulators are placed in one single hall above ground, and the high-voltage pulse is fed to the pulse transformers by up to 2-km-long cables.

Fig. 4 | View of the undulator installation in the tunnel. A 5-m-long undulator segment is shown in the front, while the 1.1m intersection with the BPM, quadrupole magnet and phase-shifter is partially hidden from view on the right side of the undulator. During operation, the complete undulator is enclosed in climate housing. Panels of the removable housing can be seen to the far right. Credit: European XFEL / Heiner Müller-Elsner

After the linac, a collimation section protects downstream hardware in case of component failure and collimates halo particles[34].

The electrons are distributed by a fast-rise-time, high-precision, flat-top strip-line kicker into one of the two electron beamlines. Another kicker system, installed upstream, is capable of deflecting single bunches into a dump beamline[35]. This configuration allows for a free choice of the bunch pattern in each electron beamline, while operating the linac with constant beam loading. Figure 3 summarizes the accelerator layout.

Commissioning of the RF system was given the highest priority in the early phase of linac operation. Proper adjustment of the many parameters of the so-called LLRF system—stabilizing the acceleration field's amplitude and phase within each RF pulse and from pulse to pulse—was achieved in a sequence of steps that had to be performed for each of the 25 RF stations[36]. Frequency tuning, RF signal checks, coupler tuning, coarse power-based calibration and closed-loop operation were achieved without the beam. After establishing beam transport—typically 30 bunches at 500 pC—cavity phasing and beam-based calibration followed. Although the first station in linac section L1 required one week of commissioning, the three stations of L2 could be handed over to operations after only one more week. Work in L3 then progressed in parallel on all available stations. The possibility to time shift the RF pulse of stations with respect to each other allowed the parallel operation of different stations for beam acceleration and RF commissioning, thus steadily increasing the available accelerating field during beam commissioning.

After the initial commissioning, each station was fine-tuned to obtain maximum performance; at present, this is at ~90% of the gradient limit obtained from previous module test results[37]. The maximum energy reached with all available stations on the beam is 17.5 GeV so far, in accordance with the design specification. User runs have been performed with 14 GeV, thus giving ample overhead for reliable linac operation.

The phase and amplitude stability of the RF pulse has been measured within the RF regulation loops to be better than 0.01° and 0.01% (ref. [38]) and thus exceeds specifications.

Measurements of the electron energy jitter give an upper limit for the r.m.s. relative energy jitter of 3×10^{-4} after the injector, 1.5×10^{-4} after BC1 and BC2 and 1×10^{-4} after the accelerator. The arrival time jitter is measured[39] to be ~20–30 fs r.m.s. after the last bunch compression stage. Energy stability and arrival time are not affected by further beam transport to the undulators, and the above values thus represent the stability to be expected at the FELs.

FEL undulators. The SASE1 FEL system consists of 35 undulator segments of 5 m length interspaced by 1.1 m sections with air coils, permanent magnet phase shifters, quadrupole magnets and electron beam position monitors (BPMs), with a total length of 213.5 m (Fig. 4). The 40-mm-period undulators are gap-tunable within a range of 10–220 mm, with an operational gap range of 10–20 mm, to enable selecting the photon energy for a given electron energy. The parameters of the SASE1 FEL undulator system are provided in Table 1.

The undulator segments and phase shifters were assembled, tested and tuned prior to installation in the tunnel. All magnetic parameters were tuned using pole height tuning[40]. Permanent magnet phase shifters are installed between undulator segments to match the phases of the electron motion and FEL radiation field. Combining the data of undulator segments and phase shifters allows determination of the gap of a specific phase-shifter for the selected K parameter of the undulator as a function of the two surrounding undulator segments[41].

A particular requirement for successful FEL lasing using gap-tunable undulators is the straightness of the electron orbit for all undulator K values. The phase-shifters are designed to have very low stray magnetic fields and first field integral errors[42,43]. To compensate for the total first- and second-field integrals of each undulator segment, each segment is equipped with a combined horizontal–vertical air coil at either end[44]. Air-coil currents are determined by moving wire measurements with an accuracy better than 0.004 T mm and 20 T mm^2, respectively[45]. Although the air coils compensate residual gap-dependent field integral errors of the

undulator segments, the overall electron trajectory is controlled by movable quadrupoles (QMs). Both air coils and QMs provide steering free of magnetic hysteresis.

The controls of the FEL undulator system use look-up tables to synchronize the phase-shifter gap and the four air coils with the gap of each of the undulator segments. Selection of the K parameter is based on the tabulated gap versus K values: the gaps were measured with a typical accuracy of $\pm 1\,\mu m$ or better. For a requested K, the gap can be adjusted such that the resulting $\Delta K/K$ over all segments of the system is less than 10^{-4}. For each K value, the required phase-shifter gap and proper air-coil currents are also taken from the look-up table. The contents of these look-up tables were initially determined through laboratory measurements of the undulator fields. Further refinement and updating using beam-based data led to further improvements.

Photon beam properties. Lasing of SASE1 at 1.3 keV was observed at an electron beam energy of 6.4 GeV during commissioning, with an undulator K parameter value of ~3.5. The estimated field gain length for these parameters is below 2 m, and thus the alignment of the electron trajectory was relaxed. Lasing was demonstrated by detecting an increase of the integrated intensity on a scintillating screen ~170 m downstream from the undulator when changing the electron peak current[46].

Crucial for lasing is the overlap of the electron trajectory with the radiation field. At a wavelength in the hard X-ray regime (above 7 keV), this requires the straightness of the trajectory to be within a few micrometres along several of the 6.1-m-long undulator cells. These tolerances cannot be achieved by standard alignment and have to be obtained by beam-based methods. Several photon- or electron-beam-based techniques exist. We chose a method based on the observation and correction of electron trajectories at different electron energies (electron beam-based alignment, eBBA)[3,47]. The initial eBBA resulted in a correction of the quadrupole centre and BPM positions of the order of 0.5 mm peak-to-peak, as had been expected for the alignment of the 213.5-m-long undulator system.

In addition to the electron trajectory, the K-value profile along the undulator (taper), the phase-shifter gap and the air-coil settings currently need to be adjusted empirically to maximize FEL intensity. Some of these time-consuming adjustments will be replaced by photon-based methods after the needed diagnostics are fully commissioned.

Photon pulse energies of up to 2 mJ between 7 and 14 keV have been achieved. The high pulse energies were reached using tapering of undulator segments.

To characterize the FEL radiation, several photon diagnostics and optics devices were used[48–50]: screens for imaging spontaneous and FEL radiation, and slits for collimating spontaneous radiation and attenuators. The absolute FEL pulse energy is measured in a calibrated ionization chamber (X-ray gas monitor, XGM) at 185 m behind the undulator. The calibrated signal is an average over several pulse trains; however, the monitor is also capable of providing the shot-to-shot pulse energies at a 4.5 MHz repetition rate within trains. At pulse energies below ~50 μJ, the XGM sensitivity is not sufficient to perform absolute measurements, but relative changes can be monitored down to the low level of spontaneous radiation of single undulator segments, which is essential for tuning for SASE lasing. Relative pulse energy measurements can also be obtained from calculating the integrated intensity on imagers.

An example of this measurement as a function of magnetic length of the undulator is shown in Fig. 5 for a photon energy of 9.3 keV. The 14 GeV electron beam has nominal parameters of 250 pC bunch charge, 5 kA peak current and a normalized slice emittance of ~0.6 mm mrad. Start-to-end beam dynamics simulations suggest a saturation length of ~80 m and an FEL pulse energy of ~600 μJ with these parameters. The measured gain curve clearly demonstrates

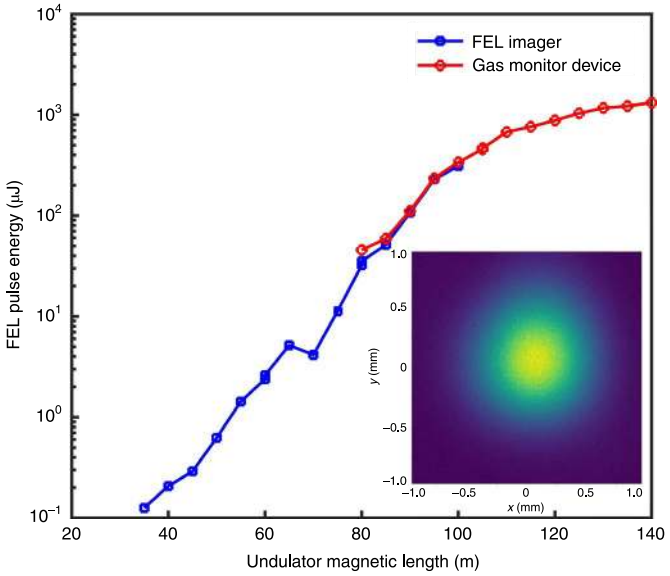

Fig. 5 | Integrated FEL pulse energy as a function of undulator magnetic length. The measurements were made with a transparent XGM (red) and an invasive FEL imager (blue). For the FEL imager, a summed image of ~1,500 trains was used for each undulator length (the inset shows a single image for 100 m undulator length). The XGM value was averaged over all trains. The FEL imager values have been normalized to the XGM value at an undulator length of 90 m.

a stage of exponential amplification and a saturation regime. The measurement yields a saturation length of ~100 m and radiation pulse energy comparable with predictions. Some 20% overhead of the saturation length is explained by practical difficulties in the optimization of the FEL process at the initial stage of amplification at low pulse energies. Analysis of the photon beam images (inset, Fig. 5) indicates that spatial properties of the radiation are in good agreement with FEL simulations based on measured values of the electron beam emittance. The measured FEL radiation properties demonstrate reasonable agreement with predicted baseline parameters[51]. However, we still observe that the fluctuation of the radiation pulse energy is mainly driven by jittering accelerator parameters. The nature and source of jittering is under study, and we believe that proper tuning of all systems of the superconducting accelerator will allow reducing fluctuations to the level of fundamental fluctuations, as has been demonstrated at FLASH[52].

Figure 6 shows the measurement of the SASE spectrum taken with the High REsolution X-ray (HiREX) single-shot spectrometer using a Si111 crystal in 333 reflection with a bending radius of 75 mm and yielding a resolution of 250 meV and a resolving power of 3.74×10^4 (ref. [53]). The HiREX is installed in the photon transport system behind a pair of X-ray offset mirrors. The measured FEL bandwidth is ~0.3% FWHM, more than twice the nominal Pierce parameter for the given machine settings (14 GeV, 500 pC, 5 kA). This broadening is not caused by electron energy jitter but is rather an indication of energy chirp in the electron beam, leading to a frequency chirp in the SASE radiation pulse.

One of the biggest assets of the European XFEL is the capability to accelerate a large number of electron bunches per RF pulse, yielding a train of up to 2,700 photon pulses. A test run with up to 500 bunches per RF pulse was performed. The relative electron energy variation over such a pulse train is ~0.01% and is ensured by proper adjustment of the LLRF parameters. In addition, a fast transverse intra-bunch train feedback system corrects residual trajectory variations within a bunch train to better than 3 μm peak-to-peak[54]. This system is also capable of correcting the pulse-to-pulse

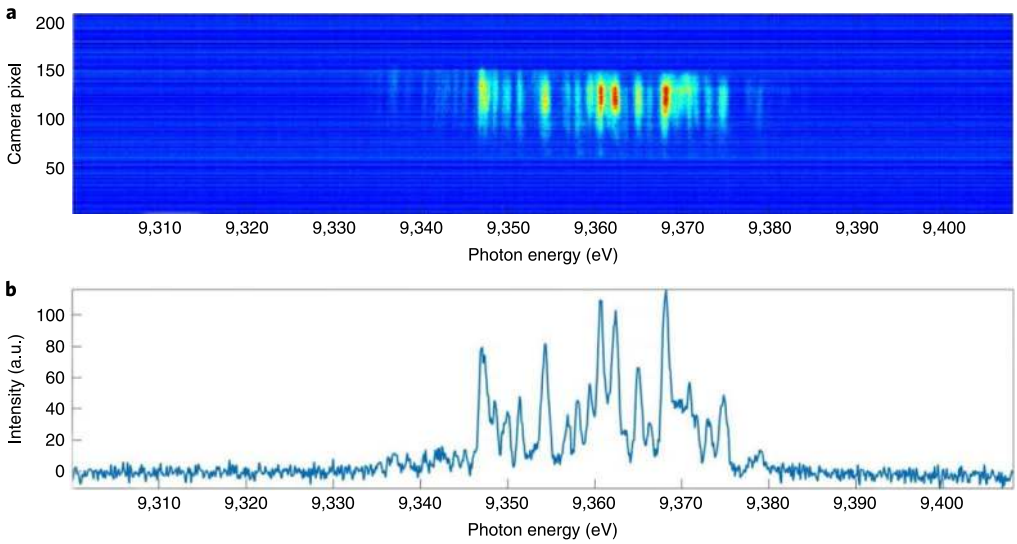

Fig. 6 | SASE spectrum measured by the HiREX single-shot spectrometer. a, Single-shot spectra collected at 9.36 keV with an electron energy of 14 GeV and 500 pC bunch charge. **b**, The line profile of the spectrum in **a**.

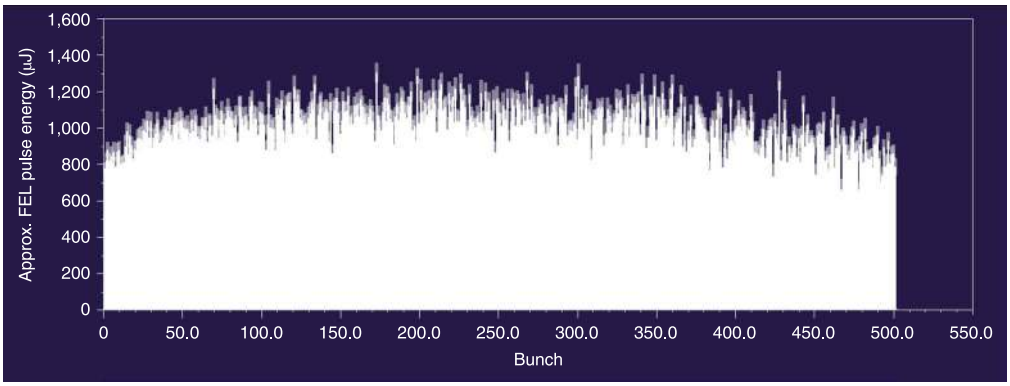

Fig. 7 | SASE FEL pulse energy measured for each X-ray pulse of a train of 500 bunches. The measurement error is indicated by the light grey parts of the bars.

transverse jitter within the same boundaries, yielding a transverse jitter of electron beam position and pointing of ~1/10 of the electron beam size. An example of the SASE1 FEL results is shown in Fig. 7, where a screen shot of the XGM data panel shows the distribution of pulse energy over a train of 500 X-ray pulses, with a total duration of 125 μs. The measured pulse energy values correspond to an average X-ray FEL power of 6 W at 9.3 keV, or even 4.8 kW throughout the X-ray pulse train. Bunch-to-bunch fluctuation of the FEL pulse energy is always expected, due to the statistical nature of SASE radiation. In addition, some modulation of the pulse energy over the train can be observed, which is attributed to very small differences in the bunch properties (energy, longitudinal profile and trajectory) within one bunch train.

In summary, we have shown the commissioning and operation results from the electron accelerator and the SASE FEL source of the European XFEL, a high-repetition-rate hard X-ray FEL facility. During this early operation of the superconducting accelerator, many target parameters have already been achieved, such as the full electron energy of 17.5 GeV or operation of the FEL at repetition rates of up to 4.5 MHz. Furthermore, the feedback mechanisms enabled by the operation of electron bunch trains provide a gain in the stability of beam position and arrival. The FEL radiation properties obtained from the SASE FEL are in good agreement with predictions of the saturated FEL radiation. Using the tapering of additional undulator segments beyond the saturation point, it becomes possible to significantly increase the FEL pulse energy. At a photon energy of 9.3 keV, using 500 bunches at 4.5 MHz per bunch train, and an average pulse energy of ~1.5 mJ, a 6 W hard X-ray FEL has been produced. The first user experiments have been performed, albeit at a reduced number of pulses per second.

Received: 30 November 2018; Accepted: 21 February 2020;
Published online: 18 May 2020

References

1. Emma, P. et al. First lasing and operation of an ångstrom-wavelength free-electron laser. *Nat. Photon.* **4**, 641–647 (2010).
2. Ishikawa, T. et al. A compact X-ray free-electron laser emitting in the sub-ångström region. *Nat. Photon.* **6**, 540–544 (2012).

3. Kang, H.-S. et al. Hard X-ray free-electron laser with femtosecond-scale timing jitter. *Nat. Photon.* **11**, 708–713 (2017).
4. Altarelli, M., Reinhard, B. & Chergui, M. *The European X-Ray Free-Electron Laser. Technical Design Report* DESY 2006-097 (DESY, 2007).
5. Ganter, R. (ed.) *SwissFEL Conceptual Design Report*, No. 10-04 (Paul Scherrer Institut, 2010).
6. Huang, Z. & Kim, K. J. Review of X-ray free-electron laser theory. *Phys. Rev. Spec. Top. Accel. Beams* **10**, 034801 (2007).
7. Pellegrini, C. The history of X-ray free-electron lasers. *Eur. Phys. J. H* **37**, 659–708 (2012).
8. Rossbach, J., Schneider, J. R. & Wurth, W. 10 years of pioneering X-ray science at the free-electron laser FLASH at DESY. *Phys. Rep.* **808**, 1–74 (2019).
9. Kondratenko, A. M. & Saldin, E. L. Generation of coherent radiation by a relativistic electron beam in an undulator. *Part. Accel.* **10**, 207–216 (1980).
10. Derbenev, Y. S., Kondratenko, A. M. & Saldin, E. L. On the possibility of using a free electron laser for polarization of electrons in storage rings. *Nucl. Instrum. Methods Phys. Res.* **193**, 415–421 (1982).
11. Murphy, J. B. & Pellegrini, C. Free electron lasers for the XUV spectral region. *Nucl. Instrum. Methods Phys. Res. A* **237**, 159–167 (1985).
12. Bonifacio, R., Casagrande, F. & De Salvo Souza, L. Collective variable description of a free-electron laser. *Phys. Rev. A* **33**, 2836–2839 (1986).
13. Hogan, M. J. et al. Measurements of gain larger than 105 at 12 μm in a self-amplified spontaneous-emission free-electron laser. *Phys. Rev. Lett.* **81**, 4867–4870 (1998).
14. Milton, S. V. et al. Exponential gain and saturation of a self-amplified spontaneous emission free-electron laser. *Science* **292**, 2037–2041 (2000).
15. Andruszkow, J. et al. First observation of self-amplified spontaneous emission in a free electron laser at 109 nm wavelength. *Phys. Rev. Lett.* **85**, 3825–3829 (2000).
16. Ackermann, W. et al. Operation of a free-electron laser from the extreme ultraviolet to the water window. *Nat. Photon.* **1**, 336–342 (2007).
17. Brinkmann, R. et al. (ed.) *TESLA Technical Design Report—Part II*: *The Accelerator*, DESY 2001-011 (DESY, 2001).
18. Brinkmann, R. et al. (ed.) *TESLA XFEL Technical Design Report*, DESY 2002-167 (DESY, 2002).
19. Grünbein, M. L. et al. Megahertz data collection from protein microcrystals at an X-ray free-electron laser. *Nat. Commun.* **9**, 3487 (2018).
20. Wiedorn, M. O. et al. Megahertz serial crystallography. *Nat. Commun.* **9**, 4025 (2018).
21. Bonifacio, R., Pellegrini, C. & Narducci, L. M. Collective instabilities and high-gain regime in a free electron laser. *Opt. Commun.* **50**, 373–378 (1984).
22. Saldin, E. L., Schneidmiller, E. A. & Yurkov, M. V. *The Physics of Free Electron Lasers* (Springer, 1999).
23. Bonifacio, R. et al. Spectrum, temporal structure and fluctuations in a high-gain free-electron laser starting from noise. *Phys. Rev. Lett.* **73**, 70–73 (1994).
24. Galayda, J. The LCLS-II: a high power upgrade to the LCLS. In *Proceedings of the 9th International Particle Accelerator Conference* 18–23 (JACoW Publishing, 2018).
25. Zhu, Z. Y. et al. SCLF: an 8-GeV CW SCRF linac-based X-ray FEL facility in Shanghai. In *Proceedings of the 38th International Free Electron Laser Conference* 182–184 (JACoW Publishing, 2017).
26. Decking, W. & Limberg, T. *European XFEL Post-TDR Description*, XFEL.EU TN-2013-004-01 (European XFEL, 2013).
27. Feng, G. et al. *Beam Dynamics Simulations for European XFEL*, TESLA-FEL 2013-01 (DESY, 2013).
28. Dwersteg, B., Flöttmann, K., Sektuowicz, J. & Stolzenburg, C. RF gun design for the TESLA VUV free electron laser. *Nucl. Instrum. Methods Phys. Rec. A* **393**, 93–95 (1997).
29. Vashenko, G. et al. Emittance measurements of the electron beam at PITZ for the commissioning phase of the European XFEL. In *Proceedings of the 37th International Free Electron Laser Conference* 285–288 (JACoW Publishing, 2015).
30. Maiano, C. et al. Commissioning and operation experience of the 3.9 GHz system in the EXFEL Linac. In *Proceedings of the 8th International Particle Accelerator Conference* 999–1002 (JACoW Publishing, 2017).
31. Hamberg, M., Brinker, F. & Scholz, M. Commissioning and first heating with the European XFEL laser heater. In *Proceedings of the 8th International Particle Accelerator Conference* 2625–2627 (JACoW Publishing, 2017).
32. Yan, M. & Gerth, C. Single-bunch longitudinal phase spaces diagnostics in multi-bunch mode at the European XFEL. In *Proceedings of the 4th International Particle Accelerator Conference* 494–496 (JACoW Publishing, 2013).
33. Brinker, F. Commissioning of the European XFEL Injector. In *Proceedings of the 7th International Particle Accelerator Conference* 1044–1047 (JACoW Publishing, 2016).
34. Balandin, V., Brinkmann, R., Decking, W. & Golubeva, N. Post-linac collimation system for the European XFEL. In *Proceedings of the 23rd Particle Accelerator Conference* 3763–3765 (JACoW Publishing, 2009).
35. Decking, W. & Obier, F. Layout of the beam switchyard at the European XFEL. In *Proceedings of the 11th European Particle Accelerator Conference* 2163–2165 (EPAC, 2008).
36. Branlard, J. et al. European XFEL RF gun commissioning and LLRF Linac installation. In *Proceedings of the 5th International Particle Accelerator Conference* 2427–2429 (JACoW, 2014).
37. Reschke, D. et al. Performance in the vertical test of the 832 nine-cell 1.3 GHz cavities for the European X-ray free electron laser. *Phys. Rev. Accel. Beams* **20**, 042004 (2017).
38. Omet, M. et al. LLRF operation and performance at the European XFEL. In *Proceedings of the 9th International Particle Accelerator Conference* 1934–1936 (JACoW, 2018).
39. Löhl, F. et al. Electron bunch timing with femtosecond precision in a superconducting free-electron laser. *Phys. Rev. Lett.* **104**, 144801 (2010).
40. Li, Y. et al. Magnetic measurement techniques for the large-scale production of undulator segments for the European XFEL. *Synchrotron Radiat. News* **28**, 23–28 (2015).
41. Li, Y. & Pflueger, J. Phase matching strategy for the undulator system in the European X-ray free electron laser. *Phys. Rev. Accel. Beams* **20**, 020702 (2017).
42. Lu, H. H., Li, Y. & Pflueger, J. The permanent magnet phase shifter for the European X-ray free electron laser. *Nucl. Instrum. Methods Phys. Rec. A* **605**, 399–408 (2009).
43. Li, Y. & Pflueger, J. Tuning method for phase shifters with very low first field integral errors for the European X-ray free electron laser. *Phys. Rev. Spec. Top. Accel. Beams* **18**, 030703 (2015).
44. Yakopov, M. et al. Automation of the magnetic field measurements of the air coils by means of the moving wire system. In *Proceedings of the 11th International Workshop on Personal Computers and Particle Accelerator Controls* 114–116 (JACoW Publishing, 2016).
45. Wolff-Fabris, F., Viehweger, M., Li, Y. & Pflüger, J. High accuracy measurements of magnetic field integrals for the European XFEL undulator systems. *Nucl. Instrum. Methods Phys. Rec. A* **833**, 54–60 (2016).
46. Decking, W. & Weise, H. Commissioning of the European XFEL accelerator. In *Proceedings of the 8th International Particle Accelerator Conference* 1–6 (JACoW, 2017).
47. Emma, P., Carr, R. & Nuhn, H. D. Beam-based alignment for the LCLS FEL undulator. *Nucl. Instrum. Methods Phys. Rec. A* **429**, 407–413 (1999).
48. Tschentscher, T. et al. Photon beam transport and scientific instruments at the European XFEL. *Appl. Sci* **7**, 592 (2017).
49. Grünert, J. et al. X-ray photon diagnostics devices for the European XFEL. *Proc. SPIE* **8504**, 85040R (2012).
50. Grünert, J. et al. First photon diagnostics commissioning at the European XFEL. *AIP Conf. Proc.* **2054**, 030014 (2018).
51. Schneidmiller, E. A. & Yurkov, M. V. *Photon Beam Properties at the European XFEL* (December 2010 revision), preprint DESY 11-152 (DESY, 2011).
52. Schneidmiller, E. A. & Yurkov, M. V. Coherence properties of the radiation from FLASH. *J. Mod. Opt.* **63**, 293–308 (2016).
53. Grünert, J. et al. Photon diagnostics and photon beamline installations at the European XFEL. In *Proceedings of the 37th International Free Electron Laser Conference* 764–768 (JACoW Publishing, 2015).
54. Keil, B. et al. Status of the European XFEL transverse intra bunch train feedback system. In *Proceedings of the 4th International Beam Instrumentation Conference* 492–496 (JACoW Publishing, 2015).

Data availability

The data that support the plots within this paper and other findings of this study are available from the corresponding author upon reasonable request.

Acknowledgements

The accelerator of the European XFEL and major parts of the infrastructure have been contributed by the Accelerator Construction Consortium, coordinated by DESY. The consortium consists of Centre National de la Recherche Scientifique – Institut National de Physique Nucléaire et de Physique des Particules (CNRS–IN2P3, Orsay, France), Commissariat à l'Energie Atomique et aux Energies Alternatives – Institut de Recherche sur les Lois Fondamentales de l'Univers (CEA–IRFU, Saclay, France), DESY (Hamburg, Germany), Istituto Nazionale di Fisica Nucleare – Laboratori Acceleratori e Superconduttività Applicata (INFN–LASA, Milano, Italy), National Centre for Nuclear Research (NCBJ, Świerk, Poland), Wrocław University of Technology (WUT, Wrocław, Poland), The Henryk Niewodniczański Institute for Nuclear Physics – Polish Academy of Science (IFJ–PAN, Kraków, Poland), Institute for High Energy Physics (IHEP, Protvino, Russia), D.V. Efremov Scientific Research Institute of Electrophysical Apparatus (NIIEFA, St. Petersburg, Russia), Budker Institute of Nuclear Physics – Siberian Branch of Academy of Science (BINP, Novosibirsk, Russia), Institute for Nuclear Research – Russian Academy of Science (INR, Moscow, Russia), Centro de Investigaciones Energéticas, Medioambientales y Tecnológicas (CIEMAT, Madrid, Spain), Universidad Politécnica de Madrid (UPM, Madrid, Spain), Stockholm University (SU, Stockholm, Sweden), Uppsala University (UU, Uppsala, Sweden) and Paul Scherrer Institute (PSI, Villigen, Switzerland). A list of members of the Accelerator Construction Consortium is provided in the Supplementary Information.

Author contributions

All authors have contributed to the design and construction of the European XFEL. W.D. wrote the manuscript draft with input from M. Yurkov., T. Tschentscher, J. Pflüger and J. Grünert. The experiments were performed by K. Appel, B. Beutner, U.B., J.B., F. Brinker, W.D., M. Dommach, W.F., L.F., G. Geloni, N. Ge., C.G., J. Grünert, M. Ilchen, M. Izquierdo, R. Ka., S. Karabekyan, A. Koch, Z.K., N. Kujala, D.L.C., Y.L., T. Limberg, D. Lipka, S. Liu, T. Maltezopoulos, M. Messerschmidt, D.N., M. Omet, I.P., L. Samoylova, D. Sanzone, E. Schneidmiller, M. Scholz, S.S., M. Sikorski, H. Sinn, S.T., T. Wamsat and P.Z.

Competing interests

The authors declare no competing interests.

Additional information

Supplementary information is available for this paper at https://doi.org/10.1038/s41566-020-0607-z.

W. Decking[1]✉, S. Abeghyan[2], P. Abramian[3], A. Abramsky[4], A. Aguirre[5], C. Albrecht[1], P. Alou[5], M. Altarelli[2], P. Altmann[1], K. Amyan[1], V. Anashin[4], E. Apostolov[6], K. Appel[2], D. Auguste[7], V. Ayvazyan[1], S. Baark[1], F. Babies[2], N. Baboi[1], P. Bak[4], V. Balandin[1], R. Baldinger[8], B. Baranasic[2], S. Barbanotti[1], O. Belikov[4], V. Belokurov[1], L. Belova[4], V. Belyakov[9], S. Berry[10], M. Bertucci[11], B. Beutner[1], A. Block[1], M. Blöcher[1], T. Böckmann[1], C. Bohm[12], M. Böhnert[1], V. Bondar[2], E. Bondarchuk[9], M. Bonezzi[11], P. Borowiec[13], C. Bösch[1], U. Bösenberg[2], A. Bosotti[11], R. Böspflug[1], M. Bousonville[1], E. Boyd[2], Y. Bozhko[1], A. Brand[1], J. Branlard[1], S. Briechle[1], F. Brinker[1], S. Brinker[1], R. Brinkmann[1], S. Brockhauser[2], O. Brovko[14], H. Brück[1], A. Brüdgam[1], L. Butkowski[1], T. Büttner[1], J. Calero[3], E. Castro-Carballo[1], G. Cattalanotto[5], J. Charrier[10], J. Chen[11], A. Cherepenko[1], V. Cheskidov[4], M. Chiodini[11], A. Chong[1], S. Choroba[1], M. Chorowski[15], D. Churanov[16], W. Cichalewski[17], M. Clausen[1], W. Clement[1], C. Cloué[10], J. A. Cobos[5], N. Coppola[2], S. Cunis[2], K. Czuba[18], M. Czwalinna[1], B. D'Almagne[7], J. Dammann[1], H. Danared[12], A. de Zubiaurre Wagner[1], A. Delfs[1], T. Delfs[1], F. Dietrich[2], T. Dietrich[1], M. Dohlus[1], M. Dommach[2], A. Donat[1], X. Dong[2], N. Doynikov[9], M. Dressel[1], M. Duda[19], P. Duda[15], H. Eckoldt[1], W. Ehsan[2], J. Eidam[2], F. Eints[1], C. Engling[1], U. Englisch[2], A. Ermakov[1], K. Escherich[1], J. Eschke[1], E. Saldin[1], M. Faesing[1], A. Fallou[7], M. Felber[1], M. Fenner[1], B. Fernandes[2], J. M. Fernández[5], S. Feuker[1], K. Filippakopoulos[2], K. Floettmann[1], V. Fogel[1], M. Fontaine[10], A. Francés[5], I. Freijo Martin[2], W. Freund[2], T. Freyermuth[2], M. Friedland[1], L. Fröhlich[1], M. Fusetti[11], J. Fydrych[15], A. Gallas[7], O. García[5], L. Garcia-Tabares[3], G. Geloni[2], N. Gerasimova[2], C. Gerth[1], P. Geßler[2], V. Gharibyan[1], M. Gloor[8], J. Głowinkowski[20], A. Goessel[1], Z. Gołębiewski[21], N. Golubeva[1], W. Grabowski[21], W. Graeff[2], A. Grebentsov[14], M. Grecki[1], T. Grevsmuehl[1], M. Gross[1], U. Grosse-Wortmann[1], J. Grünert[2], S. Grunewald[1], P. Grzegory[22], G. Feng[1], H. Guler[7], G. Gusev[4], J. L. Gutierrez[3], L. Hagge[1], M. Hamberg[23], R. Hanneken[1], E. Harms[24], I. Hartl[1], A. Hauberg[1], S. Hauf[2], J. Hauschildt[1], J. Hauser[1], J. Havlicek[1], A. Hedqvist[12], N. Heidbrook[1], F. Hellberg[12], D. Henning[1], O. Hensler[1], T. Hermann[1], A. Hidvégi[12], M. Hierholzer[1], H. Hintz[1], F. Hoffmann[1], Markus Hoffmann[1], Matthias Hoffmann[1], Y. Holler[1], M. Hüning[1], A. Ignatenko[1], M. Ilchen[2], A. Iluk[15], J. Iversen[1], J. Iversen[1], M. Izquierdo[2], L. Jachmann[1], N. Jardon[2], U. Jastrow[1], K. Jensch[1], J. Jensen[1], M. Jeżabek[19], M. Jidda[2], H. Jin[1], N. Johannson[23], R. Jonas[1], W. Kaabi[7], D. Kaefer[1], R. Kammering[1], H. Kapitza[1], S. Karabekyan[2], S. Karstensen[1], K. Kasprzak[19], V. Katalev[1], D. Keese[1], B. Keil[8], M. Kholopov[4], M. Killenberger[1], B. Kitaev[9], Y. Klimchenko[9], R. Klos[1], L. Knebel[1], A. Koch[2],

M. Koepke[1], S. Köhler[1], W. Köhler[1], N. Kohlstrunk[2], Z. Konopkova[2], A. Konstantinov[9], W. Kook[1], W. Koprek[8], M. Körfer[1], O. Korth[1], A. Kosarev[4], K. Kosiński[21], D. Kostin[1], Y. Kot[1], A. Kotarba[19], T. Kozak[1], V. Kozak[4], R. Kramert[8], M. Krasilnikov[1], A. Krasnov[4], B. Krause[1], L. Kravchuk[16], O. Krebs[1], R. Kretschmer[1], J. Kreutzkamp[1], O. Kröplin[1], K. Krzysik[19], G. Kube[1], H. Kuehn[1], N. Kujala[2], V. Kulikov[4], V. Kuzminych[4], D. La Civita[2], M. Lacroix[7], T. Lamb[1], A. Lancetov[9], M. Larsson[12], D. Le Pinvidic[7], S. Lederer[1], T. Lensch[1], D. Lenz[1], A. Leuschner[1], F. Levenhagen[1], Y. Li[2], J. Liebing[1], L. Lilje[1], T. Limberg[1], D. Lipka[1], B. List[1], J. Liu[2], S. Liu[1], B. Lorbeer[1], J. Lorkiewicz[21], H. H. Lu[25], F. Ludwig[1], K. Machau[1], W. Maciocha[19], C. Madec[10], C. Magueur[7], C. Maiano[11], I. Maksimova[9], K. Malcher[15], T. Maltezopoulos[2], E. Mamoshkina[4], B. Manschwetus[1], F. Marcellini[8], G. Marinkovic[8], T. Martinez[3], H. Martirosyan[1], W. Maschmann[1], M. Maslov[26], A. Matheisen[1], U. Mavric[1], J. Meißner[1], K. Meissner[21], M. Messerschmidt[27], N. Meyners[1], G. Michalski[22], P. Michelato[11], N. Mildner[1], M. Moe[1], F. Moglia[1], C. Mohr[1], S. Mohr[1], W. Möller[1], M. Mommerz[1], L. Monaco[11], C. Montiel[24], M. Moretti[11], I. Morozov[4], P. Morozov[1], D. Mross[1], J. Mueller[1], C. Müller[1], J. Müller[1], K. Müller[1], J. Munilla[3], A. Münnich[2], V. Muratov[9], O. Napoly[10], B. Näser[1], N. Nefedov[4], Reinhard Neumann[1], Rudolf Neumann[1], N. Ngada[1], D. Noelle[1], F. Obier[1], I. Okunev[4], J. A. Oliver[5], M. Omet[1], A. Oppelt[1], A. Ottmar[4], M. Oublaid[7], C. Pagani[28], R. Paparella[11], V. Paramonov[16], C. Peitzmann[1], J. Penning[1], A. Perus[7], F. Peters[1], B. Petersen[1], A. Petrov[1], I. Petrov[2], S. Pfeiffer[1], J. Pflüger[2], S. Philipp[1], Y. Pienaud[7], P. Pierini[11], S. Pivovarov[4], M. Planas[2], E. Pławski[21], M. Pohl[1], J. Polinski[15], V. Popov[16], S. Prat[7], J. Prenting[1], G. Priebe[1], H. Pryschelski[1], K. Przygoda[1], E. Pyata[4], B. Racky[1], A. Rathjen[1], W. Ratuschni[1], S. Regnaud-Campderros[10], K. Rehlich[1], D. Reschke[1], C. Robson[12], J. Roever[1], M. Roggli[8], J. Rothenburg[1], E. Rusiński[15], R. Rybaniec[1], H. Sahling[1], M. Salmani[1], L. Samoylova[2], D. Sanzone[29], F. Saretzki[1], O. Sawlanski[1], J. Schaffran[1], H. Schlarb[1], M. Schlösser[1], V. Schlott[8], C. Schmidt[1], F. Schmidt-Foehre[1], M. Schmitz[1], M. Schmökel[1], T. Schnautz[1], E. Schneidmiller[1], M. Scholz[1], B. Schöneburg[1], J. Schultze[1], C. Schulz[2], A. Schwarz[2], J. Sekutowicz[1], D. Sellmann[1], E. Semenov[4], S. Serkez[2], D. Sertore[11], N. Shehzad[1], P. Shemarykin[16], L. Shi[1], M. Sienkiewicz[19], D. Sikora[18], M. Sikorski[2], A. Silenzi[2], C. Simon[10], W. Singer[1], X. Singer[1], H. Sinn[2], K. Sinram[1], N. Skvorodnev[26], P. Smirnow[1], T. Sommer[1], A. Sorokin[1], M. Stadler[8], M. Steckel[1], B. Steffen[1], N. Steinhau-Kühl[1], F. Stephan[1], M. Stodulski[19], M. Stolper[1], A. Sulimov[1], R. Susen[1], J. Świerblewski[19], C. Sydlo[1], E. Syresin[14], V. Sytchev[26], J. Szuba[2], N. Tesch[1], J. Thie[1], A. Thiebault[7], K. Tiedtke[1], D. Tischhauser[1], J. Tolkiehn[2], S. Tomin[2], F. Tonisch[1], F. Toral[3], I. Torbin[4], A. Trapp[2], D. Treyer[8], G. Trowitzsch[1], T. Trublet[10], T. Tschentscher[2], F. Ullrich[1], M. Vannoni[2], P. Varela[5], G. Varghese[1], G. Vashchenko[1], M. Vasic[5], C. Vazquez-Velez[3], A. Verguet[7], S. Vilcins-Czvitkovits[1], R. Villanueva[2], B. Visentin[10], M. Viti[1], E. Vogel[1], E. Volobuev[16], R. Wagner[1], N. Walker[1], T. Wamsat[1], H. Weddig[1], G. Weichert[1], H. Weise[1], R. Wenndorf[1], M. Werner[1], R. Wichmann[1], C. Wiebers[1], M. Wiencek[19], T. Wilksen[1], I. Will[30], L. Winkelmann[1], M. Winkowski[20], K. Wittenburg[1], A. Witzig[1], P. Wlk[20], T. Wohlenberg[1], M. Wojciechowski[21], F. Wolff-Fabris[2], G. Wrochna[21], K. Wrona[2], M. Yakopov[2], B. Yang[1], F. Yang[2], M. Yurkov[1], I. Zagorodnov[1], P. Zalden[2], A. Zavadtsev[16], D. Zavadtsev[16], A. Zhirnov[1], A. Zhukov[4], V. Ziemann[23], A. Zolotov[1], N. Zolotukhina[4], F. Zummack[1] and D. Zybin[16]

[1]Deutsches Elektronen-Synchrotron (DESY), Hamburg, Germany. [2]European X-Ray Free-Electron Laser Facility GmbH, Schenefeld, Germany. [3]CIEMAT Centro de Investigaciones Energéticas, Medioambientales y Tecnológicas, Madrid, Spain. [4]Budker Institute of Nuclear Physics of the Siberian Branch Russian Academy of Sciences, Novosibirsk, Russia. [5]Universidad Politécnica de Madrid, Madrid, Spain. [6]Technical University Sofia, Sofia, Bulgaria. [7]Laboratoire de l'Accélérateur Linéaire – Centre Scientifique d'Orsay, Orsay, France. [8]Paul Scherrer Institut, Villigen, Switzerland. [9]Joint Stock Company 'D.V. Efremov Institute of Electrophysical Apparatus' (JSC NIIEFA), Saint-Petersburg, Russia. [10]CEA Saclay, Gif-sur-Yvette , France. [11]INFN Sezione di Milano – Laboratorio LASA, Segrate, Milano, Italy. [12]Department of Physics, Stockholm University, Stockholm, Sweden. [13]Jagiellonian University, Krakow,

Poland. [14]Joint Institute for Nuclear Research, Dubna, Moscow Region, Russia. [15]Wroclaw University of Science and Technology (WUST), Wroclaw, Poland. [16]Institute for Nuclear Research of the Russian Academy of Sciences, Moscow, Russia. [17]University of Łódź, Łódź, Poland. [18]Warsaw University of Technology, Warszawa, Poland. [19]Institute of Nuclear Physics, Polish Academy of Sciences (IFJ PAN), Krakow, Poland. [20]Wroclaw Technology Park, Wroclaw, Poland. [21]National Centre for Nuclear Studies (NCBJ), Otwock-Swierk, Poland. [22]Kriosystem, Wroclaw, Poland. [23]Department of Physics and Astronomy, Uppsala University , Uppsala, Sweden. [24]Fermilab, Batavia, IL, USA. [25]Institute of High Energy Physics, Beijing Shi, China. [26]IHEP, Protvino, Moscow, Russia. [27]BioXFEL STC, Buffalo, NY, USA. [28]Università degli Studi di Milano, Dipartimento di Fisica, Milano, Italy. [29]SLAC National Accelerator Laboratory, Menlo Park, CA, USA. [30]Max-Born-Institut, Berlin, Germany. ✉e-mail: winfried.decking@desy.de